Polymer 50 (2009) 3136–3144

Contents lists available at ScienceDirect

Polymer

journal homepage: www.elsevier.com/locate/polymer

Morphology, hydration, and proton transport in novel sulfonated polyimide–silica nanocomposites

Lijun Zou, Supacharee Roddecha, Mitchell Anthamatten*

Department of Chemical Engineering, University of Rochester, 250 Gavett Hall, Rochester, NY 14627, USA

ARTICLE INFO

Article history:
Received 7 March 2009
Received in revised form
30 April 2009
Accepted 2 May 2009
Available online 12 May 2009

Keywords:
Polymer composite materials
Polymer synthesis
Polymer electrolyte membranes

ABSTRACT

A series of inorganic–organic nanocomposites containing sulfonated polyimides and silica particles were synthesized. Anhydride-terminated pre-polymers were prepared, followed by introduction of reactive silanes. Casting, curing, and acidification routines lead to nanocomposites with significantly different properties compared to parent sulfonated polyimides. The presence of silica was qualitatively confirmed using energy dispersive X-ray spectrometry and studied using solid-state ^{29}Si NMR. Thermogravimetric analysis provided a more quantitative assessment of the inorganic fraction. Electron microscopy, water vapor sorption, and impedance studies were conducted to understand how silica and ion content influences morphology and proton conductivity. Ion clusters were visible following Ag^{+} staining, and silica nanoparticles were imaged in unstained samples. Silica nanoparticles significantly reduce the solubility of prepared membranes, and promote membrane hydration. For nanocomposites prepared from high molecular weight pre-polymers, silica incorporation promotes conductivity at low relative humidity. However, for nanocomposites made from low molecular weight or high ionic content pre-polymers, silica dilutes the ion concentration and lowers proton conductivity.

1. Introduction

At the heart of a fuel cell, the proton exchange membrane (PEM) must exhibit several properties such as high proton conductivity, sufficient mechanical stability, low fuel permeability, and hydrolytic stability. In addition, the production and processing of the membrane material must be cost-effective, and the membrane must be compatible with other fuel cell components. Nafion® at present is the state-of-art, industrial standard membrane. However, Nafion® is expensive, and its application is limited by environmental compatibility, fuel crossover, and failure at high temperature. Organic–inorganic composite membranes have been prepared and evaluated for PEM applications [1,2]. Incorporation of inorganic oxides such as silica [3–7], zirconium oxide [6,8] and alumina [6] into polymer matrices improves mechanical, thermal and dimensional stability [5–7], reduces electro-osmotic drag and methanol crossover, and encourages self-humidification. In the majority of these studies, the inorganic phase is not covalently coupled to the polymer phase, and in many cases, aggregation of particles occurs, and self-humidification benefits are small.

Sulfonated polyimides (SPIs) [9–16] are among several alternatives to perfluorosulfonic acid membranes. Sulfonated polyimides exhibit relatively high proton conductivity in the water-swollen state, and they exhibit good mechanical and swelling properties. Synthesis of SPIs is relatively straightforward. The typical one-pot synthesis involves polycondensation of a dianhydride with a mixture of diamines followed by thermal imidization. A fraction of diamine reagents are sulfonated prior to condensation, allowing the ionic content to be adjusted. However, the hydrolytic stability of SPIs is rather poor. Watanabe et al. incorporated aliphatic side-groups into a sulfonated polyimide ionomer to increase the imide nitrogen's electron density (and basicity), thereby lowering hydrolytic susceptibility [9,17–21]. The authors convey that careful selection and positioning of substituents can significantly improve hydrolytic stability. Also, six-membered, naphthalenic sulfonated polyimides are generally more stable than their less hydrolytically stable five-member analogs [22,23] and crosslinking can promote stability [24,25]. Despite these efforts, hydrolytic stability remains a major obstacle to realize SPI fuel cell membranes.

We have recently reported the one-pot synthesis of sulfonated polyimides that contain incompatible poly(dimethyl siloxane) segments [16]. In this study, the presence of hydrophobic siloxane segments was found to affect water uptake behavior and morphology, and ion-containing diamines were found to inhibit incorporation of siloxane chains. Water sorption studies suggested

* Corresponding author. Tel.: +1 585 273 5526; fax: +1 585 273 1348.
E-mail address: anthamatten@che.rochester.edu (M. Anthamatten).

0032-3861/$ – see front matter © 2009 Elsevier Ltd. All rights reserved.
doi:10.1016/j.polymer.2009.05.005

that siloxane chains are excluded from the ion-containing polyimide phase, and ionomer morphology was significantly altered by addition of siloxane segments. For example, siloxane-containing samples lacked the characteristic X-ray scattering ionomer peak that was observed in parent SPI materials. Despite large changes in ionomer morphology, the proton conductivity was comparable for SPI with and without siloxanes. This study raises the important question of how SPI ionomers' water uptake, morphology, and proton transport are tied together for SPIs.

The present study embodies a second approach of stabilizing dispersed morphologies to promote proton conductivity. Here, we evaluate the incorporation of silica particles into sulfonated polyimides. Sol–gel processing is employed to ensure that silica particles do not aggregate and are covalently bound to the polyimide matrix. In general, silica particles are hydrophilic [26–29] and should support membrane hydration at lower relative humidity. Also, covalently bound silica particles may act as covalent cross-links, preventing undesirable membrane dimensional changes. By controlling the extent of swelling, the inorganic nanoparticles are expected to improve hydrolytic stability and fuel cell membrane durability. To explore this idea, a series of sulfonated polyimide–silica nanocomposites were synthesized from soluble poly(amic acid) precursors functionalized with reactive silane end-groups. To preclude the loss of mechanical properties [30–32], this study focuses on materials with silica content below 20 wt%. Impedance and water sorption measurements are reported as an important step in evaluating their potential as fuel cell membranes.

2. Experimental

2.1. Materials

4,4′-Oxydianiline (ODA) (99+%), 1,4,5,8-naphthalenetetracarboxylic dianhydride (NTDA) (99%) and toluene (99%) were purchased from Aldrich; 1-methy-2-pyrrolidinone (NMP) (99.5%, anhydrous), triethylamine (TEA, 99%), benzoic acid (99%), 4,4′-diamino-2,2′-biphenyldisulfonic acid (BDSA) (70%), 3-aminopropyl trimethoxysilane (APrTEOS, 97%) and tetraethylorthosilicate (TEOS, 98%) from Alfa Aesar; hydrochloric acid (HCl, 36.9%), sodium chloride (NaCl, 100%) from J. T. Baker; dimethyl sulfoxide (DMSO) from EMD Chemicals Inc. All materials were used without further purification except NTDA, which was vacuum-dried at 170 °C for 12 h, and BDSA, which was vacuum-dried at 90 °C for 12 h, before use.

2.2. Synthesis of dianhydride end-capped SPIs

Dianhydride end-capped SPIs were prepared by using a stoichiometric balance of dianhydride and diamine monomers to result in high molecular weight polymers [11,19,33,34]. Following this reaction, a slight excess of dianhydride was added to convert any amino end-groups to anhydride end-groups as suggested in Scheme 1.

In a typical synthesis, BDSA, ODA and NMP were added to a completely dried 100 ml 3-necked flask equipped with a Dean–Stark trap and a condenser under nitrogen purge. In addition, TEA was added to improve the solubility of BDSA, and benzoic acid functioned as catalyst [35–37]. After all reagents were dissolved, stoichiometric amount of NTDA was added into the mixture. The mixture was stirred at room temperature overnight. Then toluene was added to achieve a ratio of NMP to toluene of 4:1. The solution was then heated to 80 °C for 4 h and 180 °C for 20 h. Collected water was removed from the Dean–Stark trap with toluene. Extra NTDA with benzoic acid was added after the solution was cooled down to room temperature to raise the anhydride-to-diamine stoichiometric ratio to about 1.1:1.0 [32]. The mixture was stirred at room temperature overnight and then was heated to 80 °C for 4 h and to 180 °C for 20 h again. The warm solution-containing product was poured into 200 ml acetone, and the powder precipitate was filtered, washed with acetone, and dried in vacuum oven at 120 °C overnight.

2.3. Synthesis of SPI–Si nanocomposites

The anhydride-terminated SPI product was re dissolved in NMP at 5 wt%, and APrTEOS and TEOS were added successively and each stirred for 10–15 min. Then the solution was cast under N_2 purge into a PDMS mold at room temperature for 12 h and then held and at 50 °C for 3–4 days, or until the solvent was completely evaporated. The free standing film was then soaked in 0.01 M HCl for 1 day, rinsed by DI water and cured at 120 °C overnight to complete the sol–gel reaction.

2.4. Characterization

All synthesized SPI precursors were studied using ^{1}H NMR and the resulting spectra were analyzed according to our prior study [16] (an example of an NMR spectra is provided in Supplementary Content). Molecular weights were measured via gel permeation chromatography (GPC) (Viscotek, TDA Model 301, Triple Detector Array) using NMP with LiBr (0.02 M) as the mobile phase at 60 °C and flow rate of 0.8 ml/min [16]. Free standing films (~150 μm) were studied using Attenuated Total Reflectance (ATR) mode of Shimadzu 8400S FT-IR. Thermogravimetric analysis was performed with a simultaneous DSC–TGA instrument (SDT600) at a heating rate of 10 °C/min under air. Morphologies of stained and unstained films were examined using transmission electron microscopy (TEM). Selected samples were stained by immersion in 0.1 M $AgNO_3$ aqueous solution to promote ion exchange. Samples were embedded in epoxy and microtomed to 120 nm sections. Images were acquired at 200 kV using a JEOL-2000EX TEM. Energy dispersive X-ray spectrometry (EDS) was running by an EDAX detector on a Zeiss Supra40 VP scanning electron microscopy (SEM) with a voltage of 15 kV and a working distance of 15 mm.

Solid-state magic-angle spinning (MAS) ^{29}Si NMR was performed to distinguish the following types of silicon centers: Q1 ($(SiO)Si(OH)_3$), Q2 ($Si(OSi)_2(OH)_2$), Q3 ($Si(OSi)_3(OH)$), Q4 ($Si(OSi)_4$), and T ($(SiO)_3Si$–C), by Process NMR Associates, LLC. Spectra were acquired at a resonance frequency of 39.736 MHz on a Varian UnityPlus-200 NMR spectrometer, utilizing a Doty Scientific 7 mm supersonic MAS probe. Magic-angle spinning speeds of 5 kHz were employed. Spectra were acquired using both cross-polarization (CP) and single-pulse excitation (SP) modes.

Water vapor sorption isotherms under different relative humidities (RH) were acquired using a Cahn-2000 environmental electro-balance (±1 μg) that was adapted to control humidity around the sample [16]. To ensure accuracy, the water sorption device was reset to the lowest possible relative humidity after one measurement cycle. Once the sample reached its equilibrium state, the relative humidity was set to 50% to check reproducibility. The results show our data are quite consistent and reproducible.

Water uptake results were obtained by soaking the membrane in DI water at room temperature for 24 h and calculated by the equation:

$$\text{Water Uptake} = \frac{m_{\text{wet}} - m_0}{m_0} \times 100\% \quad (1)$$

where m_{wet} and m_0 [kg] are the wet and dry masses of the membrane.

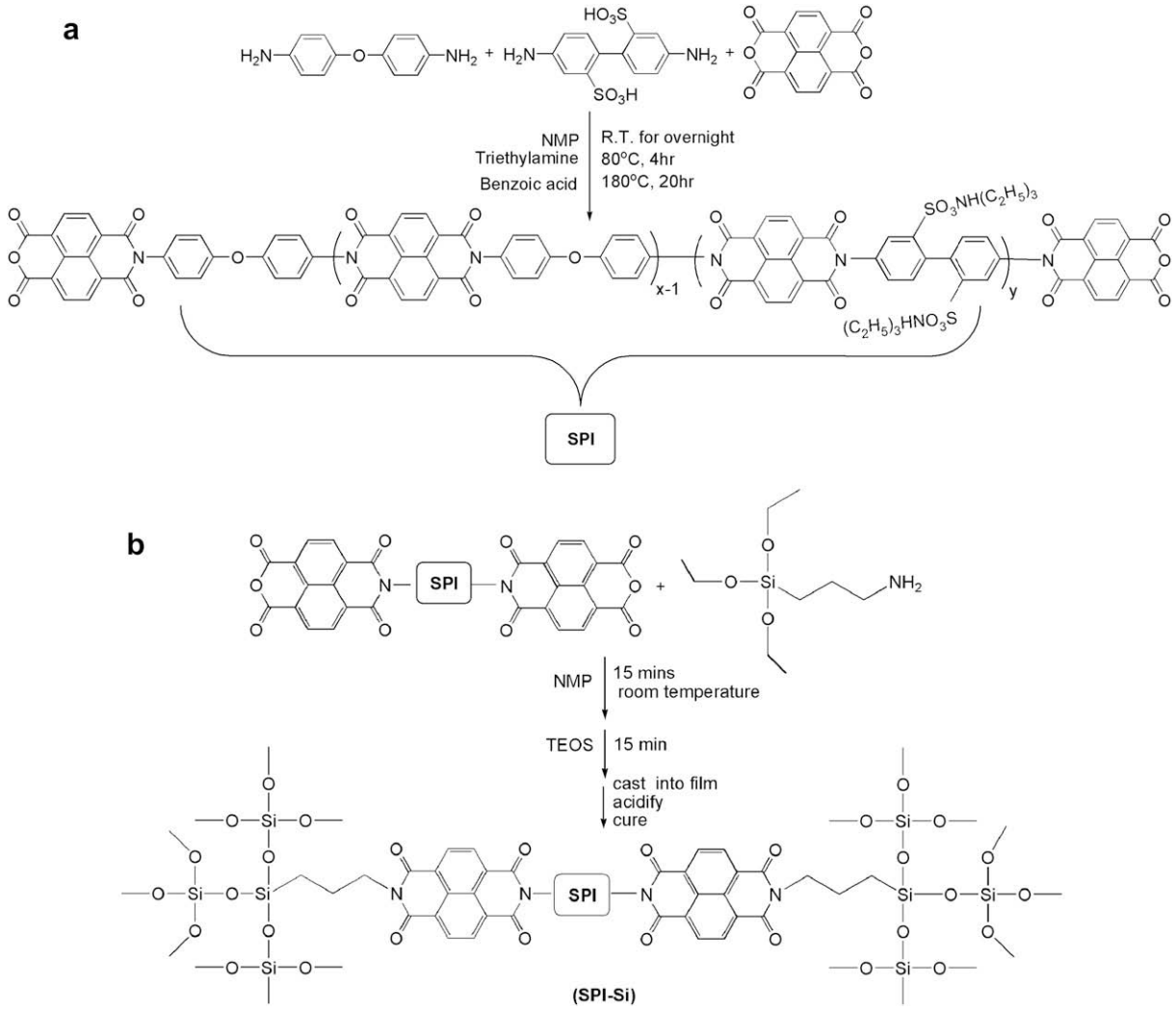

Scheme 1. Synthesis of (a) dianhydride end-capped SPI; and (b) SPI–Si nanocomposite materials.

Ion exchange capacities (IEC) were measured by soaking films (~20 mg) overnight at room temperature in 1 M HCl to ensure protonation of all sulfonic acid groups. After soaking, films were thoroughly washed with DI water several times and were ion-exchanged in 100 ml 0.1 M NaCl by soaking for 2 days. The pH value of the proton-exchanged NaCl solution was measured using a pH meter (Orion 710A plus) and the IEC [meq/g] was determined from:

$$\mathrm{IEC} = \frac{10^{-\mathrm{pH}} \times V_{\mathrm{NaCl}}}{m_0} \tag{2}$$

where V_{NaCl} [L] is the volume of NaCl solution. The proton conductivity of the membranes under different relative humidity was determined at 80 °C with a 4-point probe fuel cell test & impedance analyzer (BekkTech) over the frequency range of 1 Hz–10 KHz. Nitrogen feed gas was used at flow rate of 500 cm^3/min [16].

3. Results and discussion

Table 1 summarizes composition and key characteristics of synthesized samples. Samples are referred to as SPI_{x-y} where x denotes measured molecular weight (in kDa) and y denotes measured silica content as determined from TGA experiments. Experiments were designed to study how properties depend on molecular weight, ionic content, and silica content. Two low molecular weight SPIs were prepared that have different ionic contents, and one high molecular weight sample was prepared with low IEC. High molecular weight SPIs with high IECs could not be synthesized using our technique. The presence of a high concentration of ionic groups is known to inhibit the condensation polymerization reaction [16]. For each parent SPI, a series of nanocomposites were prepared with varying silica content.

3.1. Membrane composition and characteristics

Film-forming ability is an important property of candidate PEM materials. In general, SPIs synthesized with molecular weights higher than 10,000 g/mol with BDSA content ~30–40% exhibited good film-forming ability. The addition of silica tended to improve film-forming ability in all samples except for **SPI_{14}**. This sample is inherently more brittle, likely due to its high IEC.

Both ionic content and silica content lead to higher levels of water uptake. The water uptake in the **SPI_{26}** series, the high molecular weight series, is especially sensitive to silica content, and this will be discussed later. The solubility of silica nanocomposite materials in aprotic solvents is significantly lower than that of parent SPI materials. For example, SPI–silica materials do not dissolve in NMP, even after months, while the parent materials dissolve in just a day. This

Table 1
Feed composition, molecular weight, IEC and water uptake values of synthesized parent SPI materials and SPI-Si nanocomposites.

Sample	Parent SPI MW [g/mol]	BDSA feed composition [wt%]	Si feed composition [wt%]	IEC [meq/g]	Water uptake [wt%]	TGA (air) residue [wt%]	Film-forming ability
SPI_{15}	15,400	32	0	1.53	50.0	2.96	Excellent
SPI_{15}-4			5.0	1.37	54.4	4.13	Excellent
SPI_{15}-15			10.0	1.25	58.3	15.34	Excellent
SPI_{14}	13,600	40	0	2.21	60.0	0.67	Good
SPI_{14}-1			2.0	2.14	62.3	1.15	Good
SPI_{14}-6			5.0	1.85	60.4	6.03	Good
SPI_{14}-12			10.0	1.82	66.0	11.74	Brittle
SPI_{26}	26,300	30	0	1.78	44.6	1.14	Good
SPI_{26}-2			6.9	1.70	60.1	1.89	Good
SPI_{26}-3			5.0	1.56	62.1	3.40	Excellent
SPI_{26}-9			10.2	1.56	62.4	8.57	Excellent

suggests that silica particles have been successfully introduced, and they may be acting as covalent crosslinks.

FT-IR and EDS experiments were performed to verify the presence of silica in prepared nanocomposites. FT-IR showed a broad absorption at $\sim$1100 cm^{-1} (data provided in Supplementary Content) that may be due to Si–O–Si stretching mode. However, because this absorption overlaps with the C–H stretching band, no conclusion could be drawn. On the other hand, EDS analysis confirmed the existence of Si in the membrane. A clear silicon signal is present at 175 eV in the EDS spectrum of **SPI_{14}-12** whereas there is no signal in the parent **SPI_{14}** (Fig. 1). The Si signal does not dominate the spectrum, indicating that silica has not phase separated to the surface of the film. Moreover, EDS experiments conducted on both sides of the film appeared identical.

Thermal analysis of nanocomposites provides another indication that silica has been incorporated into the material. Fig. 2 shows thermogravimetric scans of the **SPI_{14}** series. Prior to each scan, the sample was held at 180 °C under dry air purge for 2 h to remove absorbed water. During the subsequent thermal scan, there were two stages of mass loss. The first ($\sim$300 °C) is due to loss of $-SO_3H$ groups, and the second ($\sim$550 °C) is due to the polyimide backbone degradation. A white, brittle residual mass was observed by the naked eye in sample pans following thermal scans. This inorganic material, presumed to be silica, was not observed following thermal scans of parent SPIs. However, a mass residue was observed in the TGA scan of the parent SPIs too. This recorded mass is above the resolution of the instrument and may come from the impurities introduced during the film casting, or it may be graphitic-like carbon that formed through thermal pyrolysis. With this in mind, Fig. 2 shows that, for the **SPI_{14}** series, the amount of SiO_2 residue measured was nearly proportional to the mass fraction of Si introduced during the casting procedure. The data indicate that about half of Si-containing reagents did not

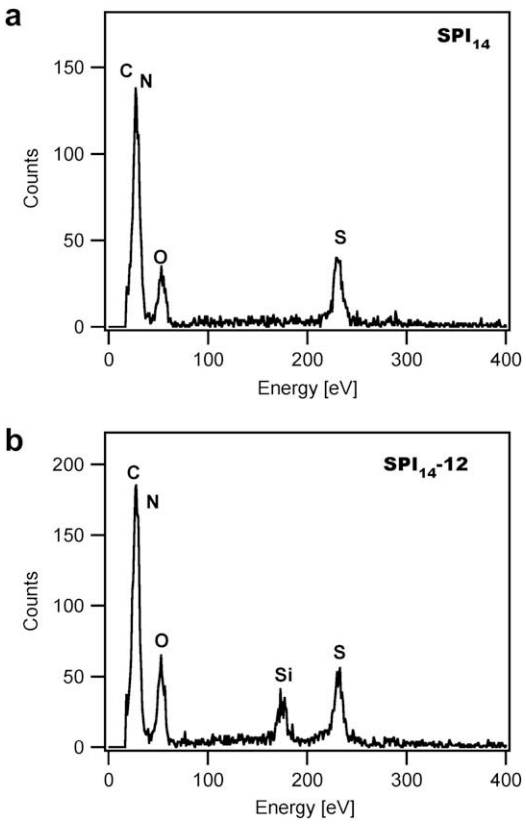

Fig. 1. EDS spectra of (a) **SPI_{14}** and (b) **SPI_{14}-12**.

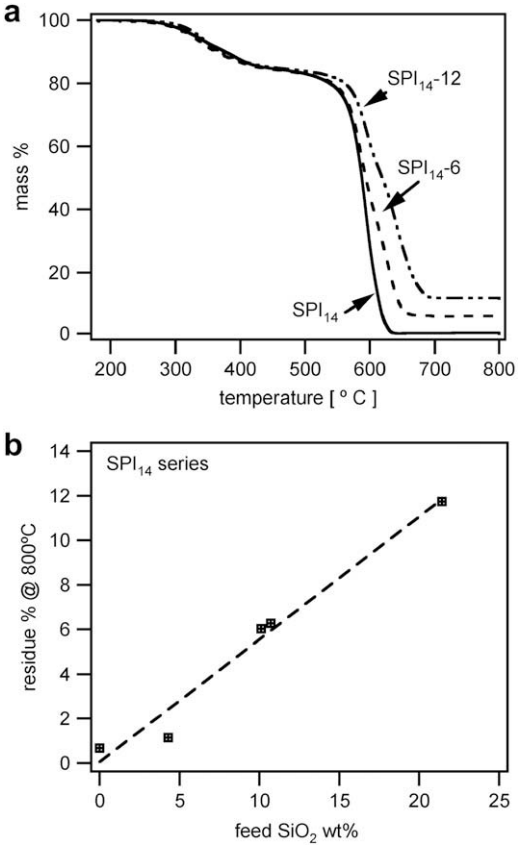

Fig. 2. Thermogravimetric analysis of SPI–Si nanocomposites: (a) thermal scans of representative samples; (b) plot of mass% residue versus SiO_2%.

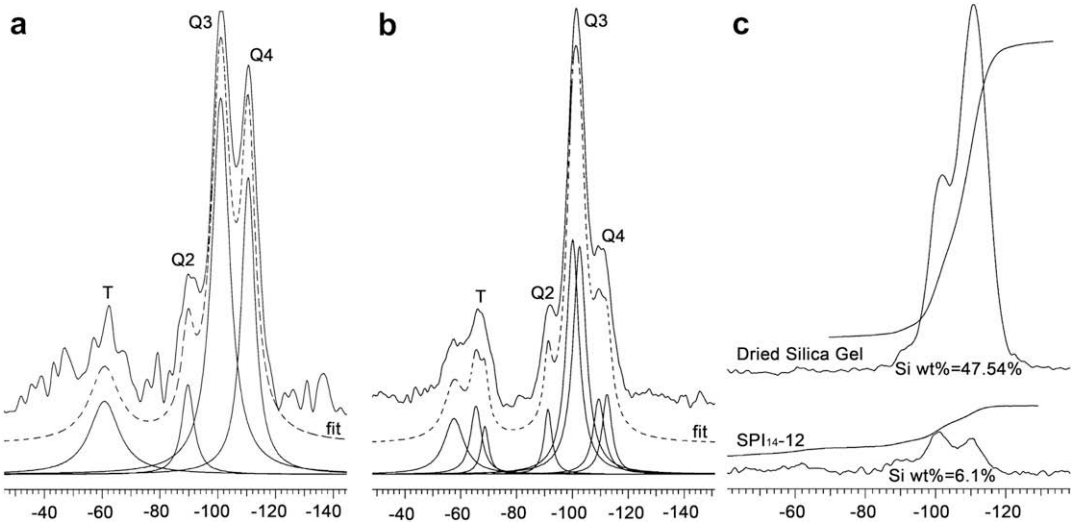

Fig. 3. Solid-state ^{29}Si NMR spectra of **SPI$_{14}$-12**: (a) single-pulse excitation spectrum; (b) cross-polarization spectrum; and (c) comparison of SP-MAS spectra of silica gel and **SPI$_{14}$-12**.

react, and were likely removed during film casting and subsequent processing. For other series, the correlation between silica feed and residual mass was somewhat weaker, and these data sets available as Supplementary Content.

Table 1 summarizes sample characteristics and lists the observed TGA mass residues. In general, the use of higher molecular weight pre-polymers resulted in lower levels of silica incorporation. This may be due to two reasons: (1) high molecular weight pre-polymers have a lower concentration of reactive anhydride end-groups, and (2) the polymer-reagent solutions show higher viscosities, that lead to more sluggish reaction kinetics.

Solid-state ^{29}Si NMR experiments were performed on a representative sample, **SPI$_{14}$-12**, to quantify the amount of Si present and to distinguish between different silicon bonding environments. This technique has been successfully applied to study several other nanocomposite systems including, for example, surfactant-templated hexagonally-ordered nanocomposites [38], sol–gel processed Zn–PEAA–silica hybrid material [39], and perfluorosulfonylfluoride nanocomposites for fuel cell membranes [40]. Prior to analysis **SPI$_{14}$-12** was washed extensively with methanol and water to any remove unreacted silanes and was acidified using HCl. Two types of magic-angle spinning (MAS) experiments were performed. In single-pulse (SP) experiments, resonances for each type of silicon species are present. These resonance peaks were integrated to provide a measure of the relative abundance of different silicon nuclei. In cross-polarization (CP) experiments ^{29}Si nuclei are only observed if they are spin-coupled to ^{1}H nuclei. For the CP experiment, a relaxation delay of 3 s was used. This time is long enough to detect spin-coupling between ^{29}Si and ^{1}H nuclei, only if they are separated by less than 7–10 Å. Detectable Si nuclei may include near-surface silanol groups and bulk silicates with branched Q3 defects. Integration of cross-polarization resonance peaks only provides a relative measure of ^{1}H coupled silicon. Comparison of the T to Q (the sum of Q1, Q2, Q3 and Q4) ratios from CP and SP experiments can indicate which silicon types are near the polyimide domains.

Table 2
Percentage of different Si states in **SPI$_{14}$-12** from single-pulse (SP) and cross-polarization (CP) excitation ^{29}Si NMR experiments.

Si state	SP-MAS(%)	CP-MAS(%)
T	15.53	21.48
Q2	7.71	4.94
Q3	47.82	57.72
Q4	28.94	15.85

Resulting single pulse (SP) and cross-polarization (CP) excitation ^{29}Si NMR spectra of **SPI$_{14}$-12** are shown in Fig. 3a and b, respectively. Si(OSi)$_4$ groups (Q4) are observed at −110 ppm, Si(OSi)$_3$(OH) groups (Q3) at −101 ppm, Si(OSi)$_2$(OH)$_2$ groups (Q2) at −91 ppm, and (SiO)$_3$Si–C (T) groups at −68 to −58 ppm. Integrated peak intensities are summarized in Table 2. Both SP and CP experiments indicate that the majority of the Si is in the form of Si(OSi)$_3$(OH) (Q3) groups. The SP spectrum shows rather low signal-to-noise ratio. This is

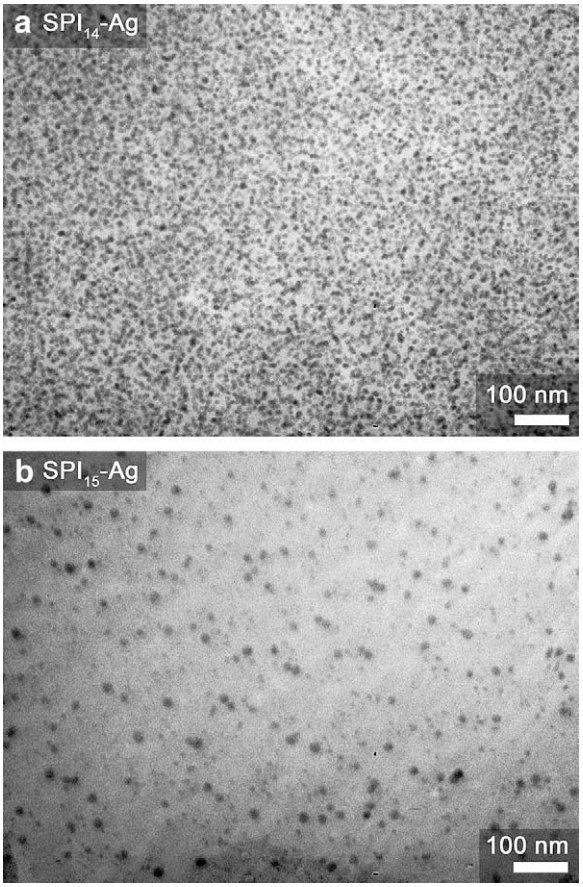

Fig. 4. TEM images of Ag^{+}-stained parent SPI materials with different IEC values: (a) **SPI$_{14}$** (Ag^{+}), IEC = 2.21 meq/g; (b) **SPI$_{15}$** (Ag^{+}), IEC = 1.53 meq/g.

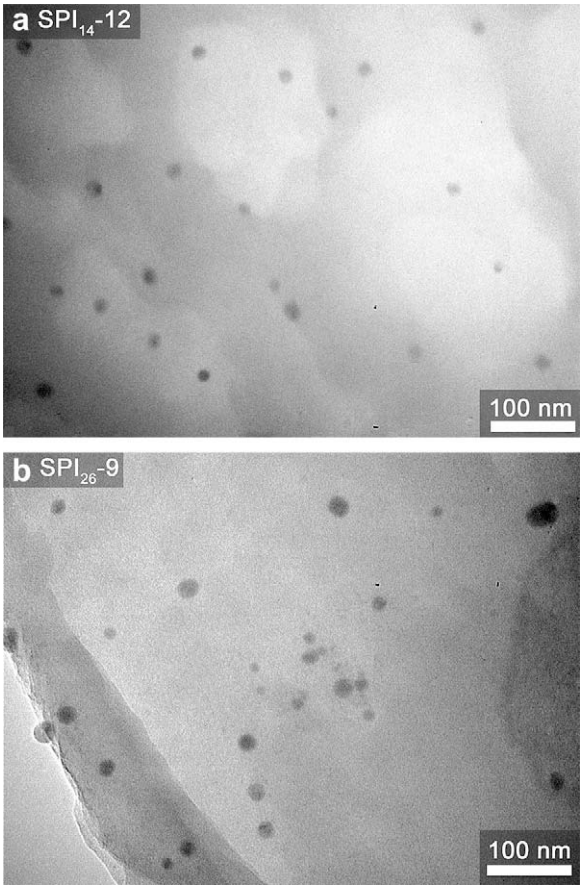

Fig. 5. TEM images of unstained SPI–silica nanocomposites: (a) low molecular weight **SPI$_{14}$-12**; (b) high molecular weight **SPI$_{26}$-9**.

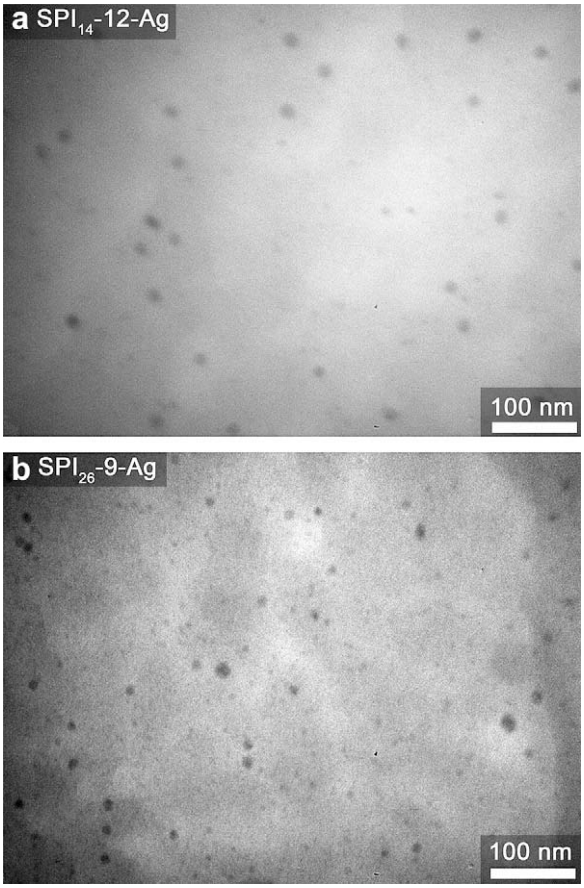

Fig. 6. TEM images of Ag^+-stained SPI–silica nanocomposites: (a) **SPI$_{14}$-12** (Ag^+), IEC = 1.82 meq/g; (b) **SPI26-9** (Ag^+), IEC = 1.56 meq/g.

attributed to the insufficiently long relaxation delay used, despite over 20 h of data acquisition. Compared to the SP experiments, CP experiments show somewhat higher relative atomic ratios of Q3 and T centers as one would expect near the silica–polymer interface.

Fig. 3c shows results from an additional SP-MAS ^{29}Si NMR experiment performed on a dried silica gel (SiO_2) containing a known amount of Si (47.54 wt%). This experiment was used to determine that **SPI$_{14}$-12** contains about 6 wt% silicon. From the SP experiment (Table 2), about 29% (relative atomic ratio) of this Si is in the Q4 form, corresponding to 3.8 wt% of SiO_2. This content is significantly lower than the residual mass observed in TGA for **SPI$_{14}$-12** (11.7%)—likely because additional hydrolysis–condensation reactions occur during the thermal cycle from 25 °C to 800 °C in the presence of air. If all Si nuclei detected using ^{29}Si NMR were converted to SiO_2 (Q4), then the expected silica mass would be 13.0%, which nearly matches the TGA result.

To summarize, ^{29}Si NMR studies are consistent with TGA studies and show that for prepared membranes, the majority of silica is covalently bond to silicate or hydrocarbon domains. Approximately one fifth of covalently bound silicon atoms are in Q4 form, and this incomplete conversion is likely due to the rather mild curing temperature (120 °C).

3.2. Membrane morphology

TEM experiments were conducted to ascertain how silica condensation affects ionomer nanoscale morphology. Selected micrographs are presented to point out major trends. Typical ionomer morphologies of synthesized parent SPIs are shown in Fig. 4. The observed contrast is a result of Ag^+ staining. Darker regions indicate ion clusters [9,16], and the lighter regions indicate non-ionic polyimide material. Fig. 4 shows that the size and number density of ionic clusters depends on the material's ionic content, similar to Watanabe's et al. study of SPIs [15,17]. For samples with low IEC, a variety of ion cluster sizes is observed, ranging from 5 to 30 nm. Ion domains tend to be smaller (<10 nm), and more closely packed, for high IEC ionomers like **SPI$_{14}$**. Well-dispersed and well-connected ionic domains are needed to promote hydration and proton transport in fuel cells.

Fig. 5 shows TEM images of two unstained, silica-containing samples. These samples have comparable ion and silica content, but differ in molecular weight. In both samples, isolated spherical particles were observed within a uniform polymer phase. These particles were not observed when unstained parent SPI (without silica) sections were studied. Therefore, the observed contrast is believed to be due to silica particles. Similar particles have been observed in unsulfonated polyimide nanocomposites [32]. The particles observed here range from 5 to 40 nm in diameter—which is somewhat larger than expected. The lower molecular weight sample, **SPI$_{14}$-12**, exhibited somewhat smaller and more monodisperse particles compared to **SPI$_{26}$-9**. This trend may be due to polyimide chain crowding at the silica surface. Assuming each polyimide chain is connected to a silica domain, the number of polymer–particle junctions is much greater for the lower molecular weight nanocomposite, and chain crowding may limit silica particle growth.

The volume fraction of dark regions in Fig. 5 does not account for the amount of silica observed using TGA and ^{29}Si NMR. This was also

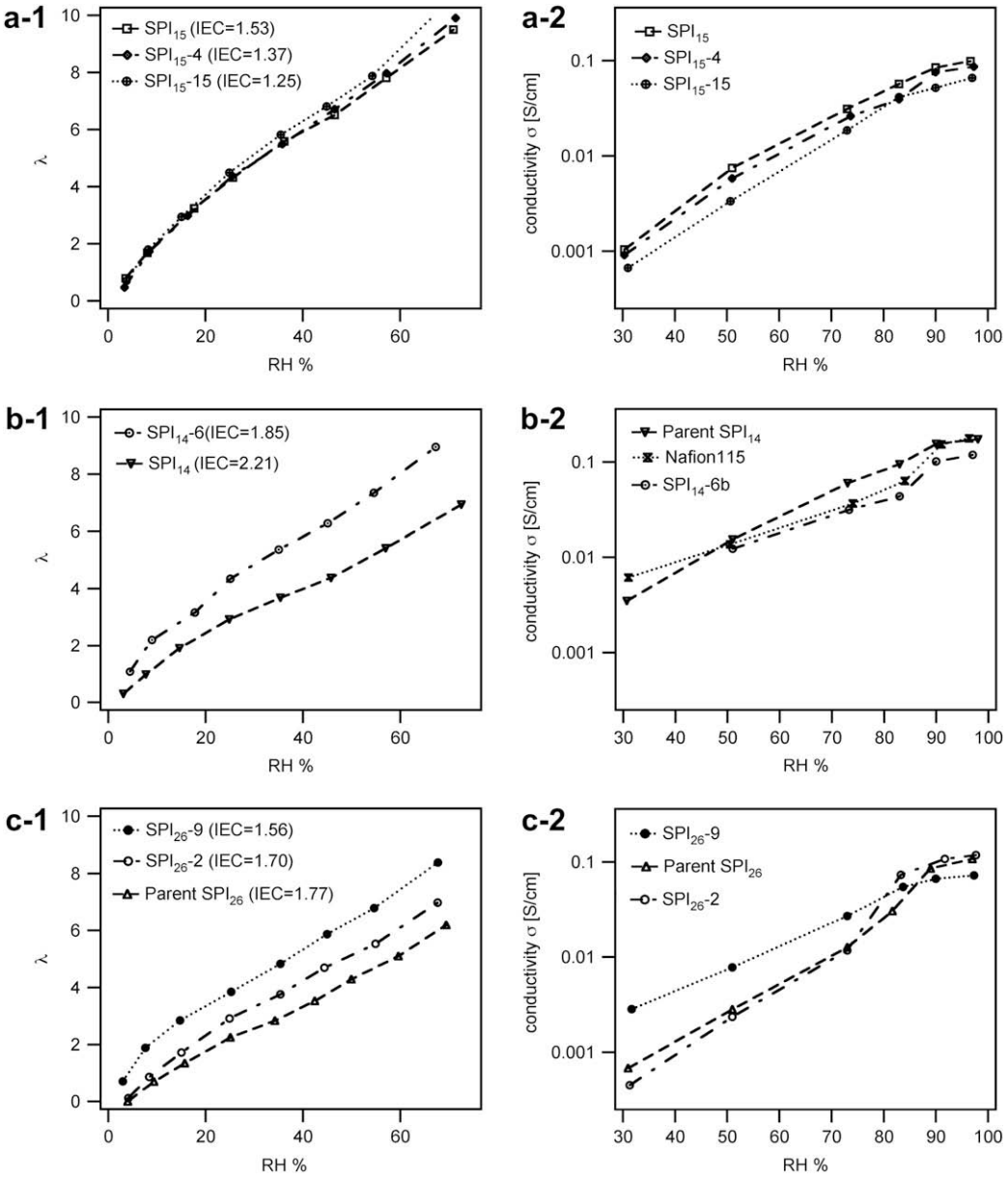

Fig. 7. Equilibrium moles of water molecules present per mole of $-SO_3H$ at different relative humidity of (a-1) **SPI_{15}**, (b-1) **SPI_{14}**, (c-1) **SPI_{26}** series; and the corresponding proton conductivities as a function of RH at 80 °C of (a-2) **SPI_{15}**, (b-2) **SPI_{14}**, (c-2) **SPI_{26}** series. Lines are drawn to guide the eye.

observed in Yen et al.'s study on unsulfonated polyimide nanocomposites [32]. If the lighter regions contain no silica, and the dark spheres are pure silica and are suspended randomly in the 100 nm sections, then a volumetric calculation suggests that samples have less than 1 wt% silica, whereas the TGA analysis suggests 11.7%. There are two ways to explain this discrepancy. First, the film casting procedure may result in silica-lean and silica-rich regions of each film, and it is possible that images were only taken of silica-lean regions. However, this explanation is unlikely because similar morphologies were observed in over 10 different film sections, and EDS data do not indicate that silica has phase separated to the surface. Another explanation is that a population of much smaller (<5 nm) silica particles may also be present which are not detectable by TEM. The single-pulse and cross-polarization ^{29}Si NMR data corroborate the latter explanation with a simple core–shell model. The core–shell model assumes the following: (1) each sphere is divided into a core region and a shell region; (2) the concentration of silicon atoms is identical in the core and the shell; (3) all silicon nuclei bound to hydroxyl groups or hydrocarbon chains (Q2 + Q3 + T) reside within the shell region, i.e. within 7 Å from the surface. The third assumption equivalently implies that the core consists of only Q4 centers, hence neglecting the possibility of bulk hydroxyl (Q3) defects. A mole balance of Q4 nuclei results in:

$$x_{tot}V_{tot} = x_{core}V_{core} + x_{shell}V_{shell} \quad (3)$$

where x_{tot} is the total Si mole fraction which are type Q4, x_{core} and x_{shell} are Q4 fractions in the core and shell, respectively, and V_{core}, V_{shell}, and V_{tot} are the volumes of different core–shell regions. The single-pulse experiment determines x_{tot} (28.94%), cross-polarization determines x_{shell} (15.85%), and x_{core} is taken to be 1.0, according to the third assumption. Since the thickness of the shell is fixed at 7 Å, equation (3) can be then solved resulting in a core radius of about 8 Å. The total sphere diameter, including the shell, would then

be 3.0 nm—to small to be detected using TEM. Moreover, since the microtomed sections are about 100 nm, there are many opportunities for silica clusters to overlap in the TEM plane-view.

Morphologies of Ag^+ stained nanocomposites are shown in Fig. 6. Remarkably, these images appear similar to the unstained images in Fig. 5. It is believed that silica particles inhibit Ag^+ transport and exchange, leading to less staining [41]. This appears to be especially true for the lower molecular weight sample **SPI_{14}-12** in Fig. 6a. On the other hand, **SPI_{26}-9** (Fig. 6b) contains both large and small features. The large features are presumably silica and the small features are likely ion clusters.

3.3. Vapor sorption and impedance characteristics

Equilibrium moisture uptake measurements were conducted over a range of relative humidity (RH) and are compared to proton conductivities in Fig. 7. In all samples studied, silica content promoted water sorption. This indicates that hydrophilic silica particles tend to draw more water into the membrane, and these results are quite consistent with the water uptake trend.

However, it is found that silica particles have varying effects in polymers with different molecular weights and IECs. When examining Fig. 7, data from a-1 can be directly compared to c-1 because they have similar IEC. This shows for **SPI_{26}**, which has a higher molecular weight, the hydration level is more sensitive to the silica content than that of **SPI_{15}**, which has a lower molecular weight. This can be explained by assuming polymer chains are grafted to silica surfaces, then, the density of chain junctions at the silica–polymer interface is lower for high molecular weight samples, compared to lower molecular weight samples. The high density of junctions in low molecular weight material may preclude water uptake, because water molecules are less able to adsorb to silica surfaces—i.e. if they are inhibited by grafted chains. However, water sorption is also affected by the IEC values of the polymer. When hydrated, a high IEC polymer will be more extended (away from the silica interface) hence providing more opportunities for water to hydrate the silica surface. Therefore, water sorption of **SPI_{14}** (Fig. 7 (b-1)) is also sensitive to silica content, and it is not fair to compare b-1 to c-1, because the IECs are very different.

Proton conductivity has been known to be directly related to the hydration and IEC of the membrane. As for the **SPI_{15}** series, incorporation of silica had the smallest effect on water uptake (Fig. 7a). However, the conductivity of these films was found to decrease with increasing silica content. This is expected because with additional silica, the material's IEC is lowered.

The parent **SPI_{14}** has a high ion content (IEC = 2.21 meq/g) and showed the highest conductivity of all samples studied. The measured conductivity of Nafion® is shown on Fig. 7b-2 for comparison. While the presence of silica particles increased λ, possibly by dispersing ion clusters, the measured conductivity decreased. In this case, the lowering of IEC in the sample containing silica (IEC = 1.85 meq/g) played a bigger role than improved hydration in determining conductivity. At lower RH, however, these effects balanced one another, and the conductivity of **SPI_{14}** and **SPI_{14}-6** nearly agreed.

Silica particles had the greatest effect on **SPI_{26}**, the high molecular weight series. The water vapor sorption curve tended toward higher values of λ as more silica was incorporated into the material. This increased water uptake associated with silica significantly improved proton conductivity at low RH, even though the material had a somewhat lower IEC. On the other hand, at high RH, enough water is already present in the membrane and the lowering of IEC plays the predominate role. This finding shows that reactive casting silica nanoparticles into SPIs may be a viable approach to solving the fuel cell water management problem.

4. Conclusions

We have successfully incorporated functionalized silanes into sulfonated polyimide pre-polymers to form SPI–Si nanocomposites. Different nanostructured morphologies have been observed in SPI–Si materials prepared from different molecular weight parent SPIs. The formation of silica was confirmed using energy dispersive spectrometry, thermogravimetric analysis, and solid-state ^{29}Si NMR. TGA experiments agree well with ^{29}Si NMR studies and reveal that the majority of silicon nuclei are covalently bonded to silicate or hydrocarbon domains. Approximately one fifth of covalently bound silicon atoms are in Q4 form, and this incomplete conversion is likely due to the rather mild curing temperature (120 °C). Silica domains are also observed using TEM, however images cannot be accurately analyzed for silica content. Water sorption studies show that silica particles encourage membrane hydration. This increased water uptake can improve proton conductivity but is also balanced by dilution of the material's ion content at high relative humidity. However, this effect varies in materials with different molecular weights and IEC values. On the other hand, the ability of silica particles to act as covalent crosslinks and inhibit hydrolytic degradation has not yet been confirmed. Our next step is to study the long-term hydrolytic stability and durability of these and other nanocomposite membranes.

Acknowledgements

The authors would like to thank the Department of Chemical Engineering at the University of Rochester for funding this project.

References

[1] Savadogo O. Journal of Power Sources 2004;127:135–61.
[2] Costamagna P, Yang C, Bocarsly AB, Srinivasan S. Electrochimica Acta 2002;47:1023–33.
[3] Jung DH, Cho SY, Peck DH, Shin DR, Kim JS. Journal of Power Sources 2002; 106:173–7.
[4] Nan C-W, Fan L, Lin Y, Cai Q. Physical Review Letters 2003;91(26): 266104-1 to 266104-4.
[5] Antonucci PL, Arico AS, Creti P, Ramunni E, Antonucci V. Solid State Ionics 1999;125:431–7.
[6] Aricò AS, Baglio V, Blasi AD, Modica E, Antonucci PL, Antonucci V. Journal of Power Sources 2004;128:113–8.
[7] Shao Z, Joghee P, Hsing I. Journal of Membrane Science 2004;229:43–51.
[8] Saccà A, gatto I, Carbone A, Pedicini R, Passalacqua E. Journal of Power Sources 2006;163:47–51.
[9] Asano N, Aoki M, Suzuki S, Miyatake K, Uchida H, Watanabe M. Journal of the American Chemical Society 2006;128:1762–9.
[10] Bai H, Ho WSW. Journal of Membrane Science 2008;313(1–2):75–85.
[11] Einsla BR, Hong Y-T, Kim YS, Wang F, Gunduz N, Mcgrath JE. Journal of Polymer Science, Part A: Polymer Chemistry 2004;42:862–74.
[12] Li Y, Jin R, Cui Z, Wang Z, Xing W, Qiu X, et al. Polymer 2007;48:2280–7.
[13] Miyatake K, Yasuda T, Hirai M, Nanasawa M, Watanabe M. Journal of Polymer Science, Part A: Polymer Chemistry 2007;45(1):157–63.
[14] Ye X, Bai H, Ho WSW. Journal of Membrane Science 2006;279:570–7.
[15] Yin Y, Yamada O, Tanaka K, Okamoto K. Polymer Journal 2006;38(3):197–219.
[16] Zou LJ, Anthamatten M. Journal of Polymer Science, Part A: Polymer Chemistry 2007;45:3747–58.
[17] Asano N, Miyatake K, Watanabe M. Journal of Polymer Science, Part A: Polymer Chemistry 2006;44:2744–8.
[18] Asano N, Miyatake K, Watanabe M. Chemistry of Materials 2004;16:2841–3.
[19] Yasuda T, Miyatake K, Hirai M, Nanasawa M, Watanabe M. Journal of Polymer Science, Part A: Polymer Chemistry 2005;43:4439–45.
[20] Yin Y, Suto Y, Sakabe T, Chen S, Hayashi S, Mishima T, et al. Macromolecules 2006;39:1189–98.
[21] Yin Y, Fang J, Watari T, Tanaka K, kita H, Okamoto K-I. Journal of Materials Chemistry 2004;14:1062–70.
[22] Fang J, Guo X, Xu H, Okamoto K-I. Journal of Power Sources 2006;159:4–11.
[23] Lee C, Sundar S, Kwon J, Han H. Journal of Polymer Science, Part A: Polymer Chemistry 2004;42:3621–30.
[24] Miyatake K, Asano N, Tombe T, Watanabe M. Electrochemistry 2007;75(2): 122–5.
[25] Park HB, Lee CH, Sohn JY, Lee YM, Freeman BD, Kim HJ. Journal of Membrane Science 2006;285(1–2):432–43.
[26] Li Q, He R, Jensen JO, Bjerrum NJ. Chemistry of Materials 2003;15(26):4896–915.

[27] Su Y-H, Liu Y-L, Sun Y-M, Lai J-Y, Wang D-M, Gao Y, et al. Journal of Membrane Science 2007;296:21–8.
[28] Lee CH, Min KA, Park HB, Hong YT, Jung BO, Lee YM. Journal of Membrane Science 2007;303(1–2):258–66.
[29] Tominaga Y, Hong I-C, Asai S, Sumita M. Journal of Power Sources 2007; 171:530–4.
[30] Chang CC, Chen WC. Chemistry of Materials 2002;14(10):4242–8.
[31] Chen Y, Iroh JO. Chemistry of Materials 1999;11(5):1218–22.
[32] Yen CT, Chen WC, Liaw DJ, Lu HY. Polymer 2003;44(23):7079–87.
[33] Miyatake K, Asano N, Watanabe M. Journal of Polymer Science, Part A: Polymer Chemistry 2003;41(24):3901–7.
[34] Shang Y, Xie X, Jin H, Guo J, Wang Y, Feng S, et al. European Polymer Journal 2006;42:2987–93.
[35] Johnson BC, Yilgor I, Tran C, Iqbal M, Wightman JP, Lloyd DR, et al. Journal of Polymer Science, Part A: Polymer Chemistry 1984;22:721.
[36] Nolte R, Ledjeff K, Bauer M, Mulhaupt R. Journal of Membrane Science 1993;83:211.
[37] Kerres J, Cui W, Reichle S. Journal of Polymer Science, Part A: Polymer Chemistry 1996;34:2421.
[38] Gray DH, Hu SL, Juang E, Gin DL. Advanced Materials 1997;9(9):731–6.
[39] Gao Y, Choudhury NR, Dutta N, Matisons J, Reading M, Delmotte L. Chemistry of Materials 2001;13(10):3644–52.
[40] Zhang LM, Xu J, Hou GJ, Tang HR, Deng F. Journal of Colloid and Interface Science 2007;311(1):38–44.
[41] Qi S, Wu Z, Wu D, Yang W, Jin R. Polymer 2009;50:845–54.